# Towards ambient temperature reversible hydrogen storage in complex hydrides: The $6Mg(NH_2)_2$ - $9LiH$ - $xLiBH_4$ (x = 1, 6, 12, 18, 24) system

**David Grant**

david.grant@nottingham.ac.uk

University of Nottingham https://orcid.org/0000-0002-6786-7720

**Nicholas Hall**

University of Nottingham https://orcid.org/0009-0005-8265-7261

**Jacob Prosser**

University of Nottingham

**Jamie Ramshaw**

University of Nottingham

**Muhammad Salman**

University of Nottingham

**Luke Woodliffe**

University of Nottingham https://orcid.org/0000-0003-1373-9528

**Sweta Munshi**

University of Nottingham

**Guillaume Esser**

Université catholique de Louvain

**Sanliang Ling**

University of Nottingham https://orcid.org/0000-0003-1574-7476

**Marek Polański**

Military University of Technology

**Yaroslav Filinchuk**

Université catolique de Louvain https://orcid.org/0000-0002-6146-3696

**Hujun Cao**

Dalian Institute of Chemical Physics

**Ping Chen**

Dalian Institute of Chemical Physics https://orcid.org/0000-0002-0625-0639

**Martin Dornheim**

University of Nottingham

Article

**Keywords:** Hydrogen Storage, Li-Mg systems, complex hydrides, hydrides, Reactive Hydride Composites, hydrogen carriers

**Posted Date:** December 24th, 2025

**DOI:** https://doi.org/10.21203/rs.3.rs-8223396/v1



**Additional Declarations:** There is **NO** Competing Interest.

# *Towards ambient temperature reversible hydrogen storage in complex hydrides: The $6Mg(NH_2)_2$ - 9LiH - $xLiBH_4$ (x = 1, 6, 12, 18, 24) system*

*Nicholas Hall [1], David Grant [1]*, Jacob Prosser [1], Jamie Ramshaw [1], Muhammad Saad Salman[1], Luke Woodliffe [1], Sweta Munshi [1], Guillaume Esser [2], Sanliang Ling [1], Marek Polanski [3], Yaroslav Filinchuk [2], Hujun Cao [4], Ping Chen [4], Martin Dornheim [1]*

*[1] – Advanced Materials Research Group, Faculty of Engineering, University of Nottingham, United Kingdom*
*[2] – Institute of Condensed Matter and Nanosciences, Université catholique de Louvain, Louvain-la-Neuve, Belgium*
*[3] – Department of Functional Materials and Hydrogen Technology, Military University of Technology, Warsaw, Poland*
*[4] – Dalian Institute of Chemical Physics, Chinese Academy of Sciences, China*
** – Corresponding author.* david.grant@nottingham.ac.uk

**Abstract:**
Hydrogen storage remains a key challenge for widescale adoption of hydrogen as an energy vector. Lightweight complex hydrides offer high storage densities but suffer from hydrogen release/cyclability above the temperatures required for practical use. Here, we report on exciting novel discoveries in ternary Reactive Hydride Composites (RHCs). We systematically tuned the $LiBH_4$ content in the well-established $Mg(NH_2)_2$ - LiH framework, achieving reversible hydrogen release at temperatures starting as low as 350 K (77 ˚C) and a capacity of 3.1 wt%; a decrease of 100 K compared to the $Mg(NH_2)_2$ - LiH system.

This is a crucial step towards the use of complex hydride-based hydrogen carriers for stationary and onboard hydrogen storage applications at ambient temperatures. These results offer insight into the reaction pathways in these RHCs and new insights for the design of next-generation solid-state hydrogen storage materials.

**Key words:** Hydrogen Storage, Li-Mg systems, complex hydrides, hydrides, Reactive Hydride Composites, hydrogen carriers

## 1. Introduction:

The transition to a low-carbon economy hinges on scalable solutions for clean energy storage and distribution, particularly in sectors where direct electrification is impractical. Hydrogen ($H_2$) holds significant potential as a clean energy vector due to its high energy content (120 mJ $kg^{-1}$ [1]) and clean combustion, offering pathways to decarbonise transport, industry, and power generation. Its use in fuel cells [2] and internal combustion engines [3] makes hydrogen a flexible alternative to fossil fuels. However, the deployment of hydrogen technologies is fundamentally constrained by storage and delivery challenges.

Conventional hydrogen storage methods, including compressed gas (> 350 bar) and cryogenic liquid hydrogen, impose energy penalties and raise safety concerns [4]. Solid-state hydrogen storage offers an appealing alternative by increasing volumetric density without the need for extreme pressures or cryo-temperatures [5]. Metal hydrides have been extensively studied as potential solid-state hydrogen storage, however poor gravimetric capacities for hydride systems, such as 1.4 wt % for $LaNi_5$ [5,6], have limited their practical use in mobile applications. To compete with battery technologies, which typically achieve system level energy densities of ca. 0.2 kWh/kg, [7] consideration of the whole system (hydride tank and fuel cell) is needed. A simple calculation demonstrates that a typical commercial car (90 – 150 kW) with a fuel cell weighing 250 kg, operating at 60% efficiency [8], supplied with 5 kg of hydrogen from a hydride of 3 wt% contained in a tank where two-thirds of the mass is structural, yields a comparable

energy density of ca. 0.2 kWh/kg. Allowing for future fuel cells weight reduction to 150 kg only increases this to a 0.25 kWh/kg system. Thus, to make a step change, hydrides must operate at near ambient temperatures and have a reversible capacity of at least 3 wt%. Currently battery technologies are pushing to reach a system energy density of ca. 0.3 kWh/kg. For a fuel cell and tank to be competitive with these battery targets, they would require the reversible capacity of the materials to be closer to 4 wt%.

Complex hydrides, including alanates (e.g., $NaAlH_4$ [9]) and borohydrides (e.g., $LiBH_4$ [10]) offer higher hydrogen capacities than intermetallic hydrides or physisorption materials [10], whilst also offering tuneable thermodynamic properties. However, their practical use is hindered by thermodynamic and kinetic limitations. For instance, $LiBH_4$ can theoretically desorb 18.5 wt%, however only 13.9 wt% hydrogen release is observed experimentally starting at 573 K, requiring temperatures as high as 873 K to reach just 9 wt% capacity [11]. The reversibility of $LiBH_4$ is equally challenging, needing 873 K and 350 bar of hydrogen for rehydriding [12,13]. Other promising materials, such as $Mg(NH_2)_2$ and LiH, have similarly high-temperature desorption profiles or produce undesirable byproducts such as ammonia [14–16].

These limitations have prompted extensive research over the last 20 years into strategies for modifying the hydrogen release and uptake behaviour of complex hydrides. Approaches such as nanoscaling [17], catalyst doping [12,18–20], and compositional tuning have yielded promising improvements, yet often with trade-offs in capacity or stability through cycling [16]. Among these efforts, the formation of multicomponent systems, known as reactive hydride composites (RHCs), have emerged as a powerful route to circumvent intrinsic kinetic and thermodynamic barriers while leveraging the favourable storage potential of complex hydrides. RHCs combine multiple hydrogen-containing phases that undergo cooperative reactions, lowering dehydrogenation enthalpies and enhancing reversibility [21–23]. The RHC approach trades some theoretical hydrogen capacity for improved kinetics, system cyclability, and practical viability through operating temperatures closer to the operating temperature of a fuel cell [24,25].

Binary RHC systems such as $MgH_2$-$LiBH_4$ (ca. 9.8 wt % $H_2$ release) [19,26–29], $Mg_2NiH_4$-$MgH_2$ (ca. 4.8 wt % $H_2$ release)[30], $Mg(NH_2)_2$ - LiH (ca. 5.6 wt % $H_2$ release) [31–37], and $Mg(NH_2)_2$ - $LiBH_4$ (ca. 11 wt % $H_2$ release) [38] have been investigated for their favourable hydrogen storage properties. Among these, the Mg–Li–N–H system in a 1:2 molar ratio ($Mg(NH_2)_2$:LiH) stands out due to its low onset dehydrogenation temperature (140 °C) and moderate theoretical reaction enthalpy of ~40 kJ $mol^{-1}$ $H_2$ [39]. The system proceeds via a solid-state reaction forming the mixed-metal imide $Li_2Mg(NH)_2$ (Equation 1):

Equation 1: $Mg(NH_2)_2 + 2LiH \rightleftharpoons Li_2Mg(NH)_2 + 2H_2$

This solid-state reaction enables reversible hydrogen storage over multiple cycles [40], although there is release of $NH_3$ from side reactions which lead to degradation of capacity over time [41]. The equilibrium-based reaction pathway promotes faster hydrogen release and uptake compared to systems reliant on single-component phase transitions, while also mitigating the kinetic limitations often associated with complex hydrides.

Furthermore, the ability to pre-synthesise the ternary imide $Li_2Mg(NH)_2$ has facilitated mechanistic studies and kinetic optimisation, revealing opportunities to tailor reaction rates and cycling behaviour as shown in recent work by Cao et al. [39] which explored synthesis of the 1:2 system from magnesium waste.

Despite the favourable thermodynamics, the practical application of systems such as this has been constrained by sluggish kinetics. Specifically, the $Mg(NH_2)_2$-LiH system has been shown in numerous studies to exhibit a relatively high activation energy for hydrogen desorption of 127 kJ $mol^{-1}$ [31,40,42,43], which significantly limits hydrogen release at moderate temperatures (below 373 K).

To address this, researchers have explored modifying the Mg–Li–N–H system by incorporating borohydrides such as $LiBH_4$. Hu et al. demonstrated that small additions of $LiBH_4$ (≤ 0.3 molar equivalents) weaken N-H bonds via in-situ chemical interactions, reducing activation barriers and enhancing sorption rates [44]. Similarly, Zhang et al. reported that incorporating a small amount of $Mg(BH_4)_2$ and $LiBH_4$ into the $Mg(NH_2)_2$ - LiH system alters the reaction pathway. Interestingly, this addition highlighted that the 6-9 ratio of $Mg(NH_2)_2$ – LiH was favoured over the 1:2 ratio, resulting in the formation of $Li_2Mg_2(NH)_3$ and $LiNH_2$ [45] (Equation 2):

Equation 2: $6Mg(NH_2)_2 + 9LiH \rightleftharpoons 3LiNH_2 + 3Li_2Mg_2(NH)_3 + 9H_2$ or $2Mg(NH_2)_2 + 3LiH \rightleftharpoons LiNH_2 + Li_2Mg_2(NH)_3 + 3H_2$

These findings highlight the sensitivity of complex hydride systems to stoichiometric and compositional changes, suggesting that tuning the $LiBH_4$ content could further optimise both thermodynamics and kinetics.

Recent studies have shown that increasing $LiBH_4$ concentrations in $Mg(NH_2)_2$–LiH–$LiBH_4$ composites significantly accelerates hydrogen uptake and release. Among the studied *y*$Mg(NH_2)_2$-*z*LiH-*x*$LiBH_4$ systems are the 6-9-1 and 6-9-12 composites, which demonstrate rapid dehydrogenation, completing hydrogen release within approximately 10 minutes at temperatures near 453 K [21,22,46]. For the 6-9-1 composition, a proposed reaction mechanism has been outlined by Zhang et al. [45], indicating that $LiBH_4$ not only participates in hydrogen release but also plays a role in the formation of stable products (Equation 3):

Equation 3: $6Mg(NH_2)_2 + 9LiH + LiBH_4 \rightleftharpoons Li_4(BH_4)(NH_2)_3 + 3Li_2Mg_2(NH)_3 + 9H_2$

Notably, the 6-9-1 system begins to desorb hydrogen at 447 K, while the 6-9-12 variant exhibits limited hydrogen release from temperatures as low as 363 K [21]. The latter system achieves a dehydrogenation enthalpy of just 24 kJ $mol^{-1}$ $H_2$, well within the 2025 U.S. DOE target range for onboard hydrogen storage applications [47]. Despite these improvements, kinetic barriers still limit the full exploitation of their thermodynamic potential, with reasonably fast (< 10 minutes) hydrogen release rates below 100 °C remaining unattainable under practical conditions [21]. These results illustrate both the progress and ongoing challenges in engineering RHC systems that simultaneously meet thermodynamic and kinetic performance benchmarks.

In this study, we investigate the influence of the $LiBH_4$ ratio on dehydrogenation in the 6$Mg(NH_2)_2$-9LiH-*x*$LiBH_4$ systems (*x* = 1, 6, 12, 18, 24), in particular focussing on new compositions and reaction pathways with high ratios of $LiBH_4$, with the aim of optimising the thermodynamics and kinetics of these RHC systems. Using a combination of thermogravimetric analysis, differential scanning calorimetry, mass spectrometry and temperature-ramped Synchrotron Powder X-ray Diffraction, we identify partial melt-like behaviour that appears to play a critical role in hydrogen release. Additionally, increased $LiBH_4$ content appears to hinder $NH_3$ release, addressing a key challenge in N-containing hydride systems. Notably, our findings demonstrate that the 6-9-18 system can desorb 3.1 wt% $H_2$ from 350 K, a significant improvement over previously reported RHCs. These insights provide new perspectives on phase

evolution and reaction mechanisms in RHCs, highlighting the potential for further performance enhancements.

## 2. Methods:

### *2.1 Preparation of 6-9-x samples:*

All materials were handled under argon atmosphere in an MBraun glovebox with $O_2$ and $H_2O$ levels below 0.1 ppm. LiH and $LiBH_4$ (≥95% purity, Merck) were used as received. $Mg(NH_2)_2$ was synthesised following the method of Cao et al. [40]: $MgH_2$ was ball-milled using reactive milling [48] under 7 bar $NH_3$ for 8 hours, followed by heating to 310 °C under static $NH_3$ (7 bar). The resulting $Mg(NH_2)_2$ had a purity of >95% (see Supplementary Information).

Reactive hydride composites were prepared with molar ratios of $Mg(NH_2)_2$:LiH:$LiBH_4$ of 6:9:*x* (*x* = 1, 6, 12, 18, 24). Each batch comprised 1.2 g of sample ball-milled with twenty-four 9 mm stainless steel balls (316L grade) in a Fritsch P6 planetary mill using a custom reactive vial [49]. Milling was conducted under 1 bar Ar, at 60:1 ball-to-powder ratio, in 2-minute cycles with 1-minute rests for 235 repetitions, alternating direction to limit overheating.

### *2.2 Thermodynamic measurements*

Thermal behaviour was assessed using TGA-DSC-MS (Setaram Setsys 1750 CS Evolution) with a Hiden HPR-20 QMS for gas analysis. Approximately 7 mg of sample was loaded into pierced-lid aluminium crucibles. Complementary DSC measurements were performed on a Netzsch STA 204 HP, using between 1-2 mg of sample in ceramic crucibles sealed in aluminium pans (pierced immediately before measurement).

All thermal experiments were performed under flowing high-purity argon (Pureshield, 99.998%, BOC) at 50 mL $min^{-1}$ for TGA-DSC-MS and 100 mL $min^{-1}$ for DSC. A heating rate of 2 K $min^{-1}$ was applied from 298 K to 500 K, chosen to optimise the resolution of sequential reaction events while ensuring consistency across sample measurements.

### *2.3 Structural characterisation techniques*

In-situ synchrotron powder XRD was performed at the ID22 beamline (ESRF, Grenoble), using a 2D PerkinElmer detector and a monochromatic beam (λ = 0.35472752 Å) for fast acquisition and high resolution [50]. Data was collected over 0–30° 2θ with a 0.03° step size. Samples were prepared in 0.7 mm borosilicate capillaries within the ESRF glove box and sealed onto spinners using epoxy glue. Prior testing confirmed no interaction between samples and capillaries (see Supplementary Information).

2D images were integrated to 1D patterns using Fit2D [51]. Temperature control was achieved via an Oxford Cryostream, with heating rates matching thermal analysis (2 K $min^{-1}$). Refinements were conducted using FullProf [52].

## 3. Results

### *3.1 Hydrogen storage properties*

Thermal analysis of the 6-9-*x* systems (*x* = 1, 6, 12, 18, 24) was performed using TGA-DSC-MS under argon flow. All samples exhibited multiple hydrogen release steps (Figure 1). For the 6-9-18 system, the first hydrogen release occurred at 350 K. All samples except the 6-9-1 showed a major hydrogen release and corresponding mass loss below 450 K, with the 6-9-18 system showing major hydrogen release at 422 K. Two additional major mass loss events were observed at 500 K and 625 K across the samples, corresponding to further hydrogen release. These later events likely involve the decomposition of excess $LiBH_4$ and formation of thermodynamically stable phases such as $Mg_3N_2$ (SI Figure 6).

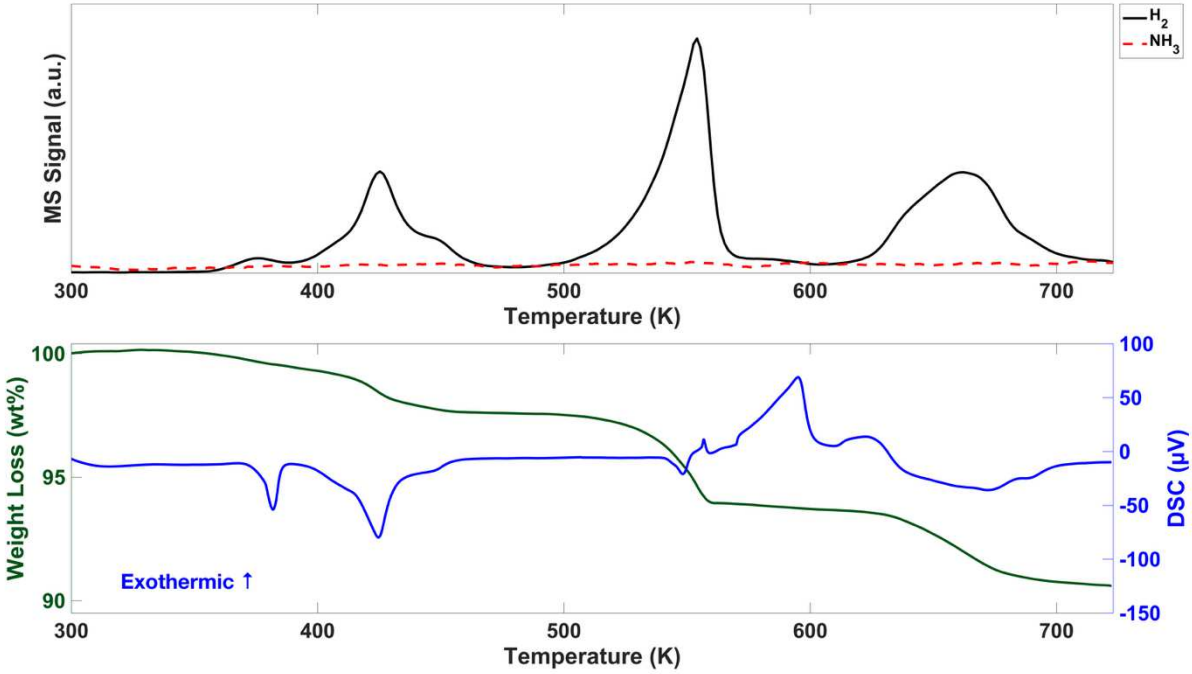


*Figure 1: TGA-DSC-MS combined plot, illustrating the complex dehydrogenation reactions of the 6Mg(NH$_2$)$_2$-9LiH-18LiBH$_4$ RHC between 298 K and 723 K at a ramp rate of 2 K per minute. 3 distinct weight loss zones are present, 298 K to 475 K, 500 K to 560 K and 630 K to 700 K. No NH$_3$ is detected above background levels in this sample.*

Within the operationally relevant temperature range of 298 to 500 K, the systems exhibited gravimetric capacities between 2.66 wt% (6-9-12) and 4.40 wt% (6-9-6), aligning with values reported in prior studies [21,22] . Notably, the 6-9-18 and 6-9-24 systems achieved higher capacities (3.12 and 2.97 wt%, respectively) compared to the 6-9-12 (2.66 wt%), despite the increased $LiBH_4$ content. Figure 2 shows that for the 6-9-6 and 6-9-18 samples, minor mass losses occur below 350 K. However, detectable hydrogen evolution begins from 350 K in the 6-9-18 system and from 385 K in the 6-9-6 system.

Compared to previous literature at an identical heating rate, the 6-9-1 system showed the peak hydrogen release at 444 K, slightly lower than the 453 K reported by Gizer et al.[22]. In the 6-9-12 system, the peak $H_2$ release occurred at 437 K, similar to prior reports of 440 K [21], with the initial $H_2$ release at 368 K again close to the 363 K previously reported. Figure 2 highlights the fact that both the 6-9-18 and 6-9-24 compositions exhibit measurable $H_2$ evolution, beginning at 350 K and 358 K respectively. Mass loss in the TGA is observed from approximately 348 K in the 6-9-6 and 6-9-18 samples. No ammonia release was detected by MS within the 298–500 K range

for the 6-9-12, 6-9-18, or 6-9-24 systems, while weak $NH_3$ signals were observed in the 6-9-1 and 6-9-6 samples, which may result in the larger gravimetric capacities.

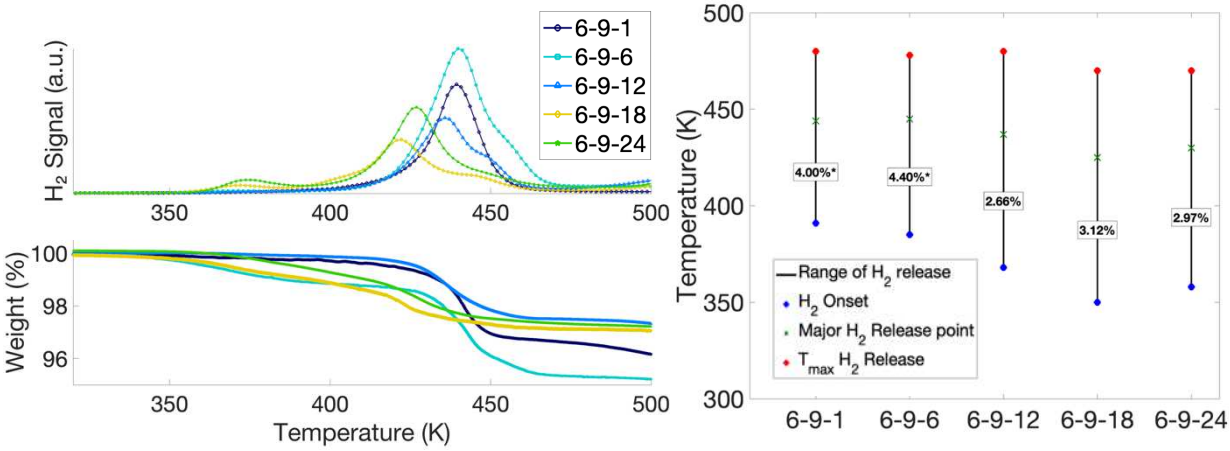


*Figure 2: (Left) TGA-MS data, highlighting the difference in reaction of the 6-9-18 and 6-9-24 samples against the previously studied 6-9-1,6-9-6 and 6-9-12 systems. (Right) A graphic visualisation of the TGA-MS data illustrating gravimetric capacities (TG), detectable $H_2$ onset temperatures (MS), major release point and temperature range. Major $H_2$ release is calculated from the derivative of the TG data, highlighting the area of steepest weight loss. * Indicates kinetic challenges in these systems from the literature*

The DSC data is indicative of the complexity of the reactions occurring between 298 K and 500 K, with multiple reactions present and clear disparities between the systems (Figure 3). All systems except 6-9-1 displayed a first endothermic event near 380 K. The enthalpies calculated from peak integration were 74.2 J $g^{-1}$ for the 6-9-18 system and 35.8 J $g^{-1}$ for the 6-9-12 system. These values were substantially higher than predicted for the $LiBH_4$ phase transition alone. In

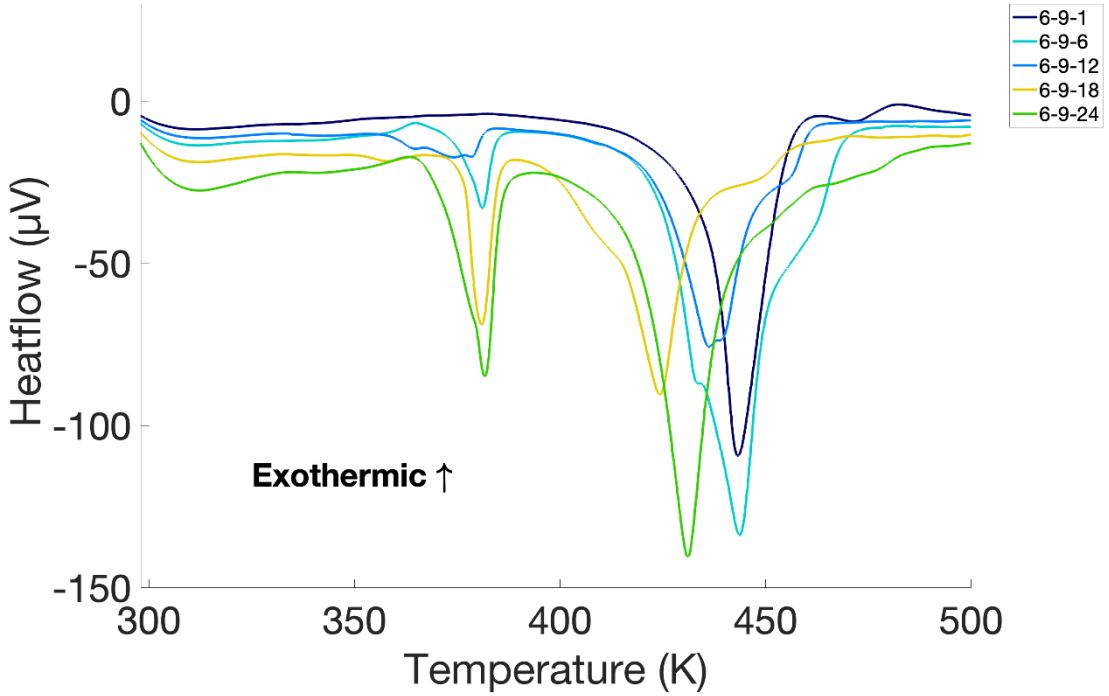


*Figure 3: DSC data of the 6-9-x (x=1,6,12,18,24) systems from 298 K to 500 K at 2 K per minute*

the 6-9-12 system, the first endothermic event appeared to consist of multiple overlapping features. The second endothermic peak, corresponding to the main hydrogen release, occurred at 422 K for the 6-9-18 system and at 437 K for the 6–9–12 system.

### *3.2 Structural evolution through dehydrogenation*

Temperature-ramped synchrotron powder X-ray diffraction (PXRD) revealed significant structural evolution in all systems (Figures 4-6). In the 6-9-1 system, diffraction peaks corresponding to $Li_2Mg_2(NH)_3$ and $Li_4(BH_4)(NH_2)_3$ formed during heating at 450 K, consistent with prior studies [22].

For the 6-9-6, 6-9-12, 6-9-18, and 6-9-24 systems, a broad low-angle peak at $2\theta \approx 1.3°$ was observed (Figure 4). This peak was present even at room temperature after milling the composites before dehydrogenation, albeit weakly, and intensified with heating, correlating with hydrogen release. In the 6-9-6 system, this peak initially grew but diminished at higher temperatures as more stable crystalline products formed. In the 6-9-18 and 6-9-24 systems, the low-angle peak persisted at elevated temperatures.

At 500 K, diffraction patterns from the 6-9-18 and 6-9-24 systems showed broad signals and minimal crystalline reflections apart from the low-angle peak (at 1.3° $2\theta$) and weak $Pm\bar{3}m$ reflections corresponding to a cubic phase with a lattice parameter of ~3.02 Å. The broad signal is across the $LiBH_4$ peaks from 420 K to 500 K, suggesting the formation of nanocrystalline, molten or amorphous products at high temperatures.

The $LiBH_4$ orthorhombic-to-hexagonal phase transformation was observed at ~390 K in all systems containing $LiBH_4$, consistent with previous studies [19,20,22,53]. However, aside from this transition, in the $x$ = 12, 18 and 24 systems limited new structural phases were detected in the diffraction patterns, suggesting the formation of amorphous, molten or poorly crystalline products as the $LiBH_4$ content increases.

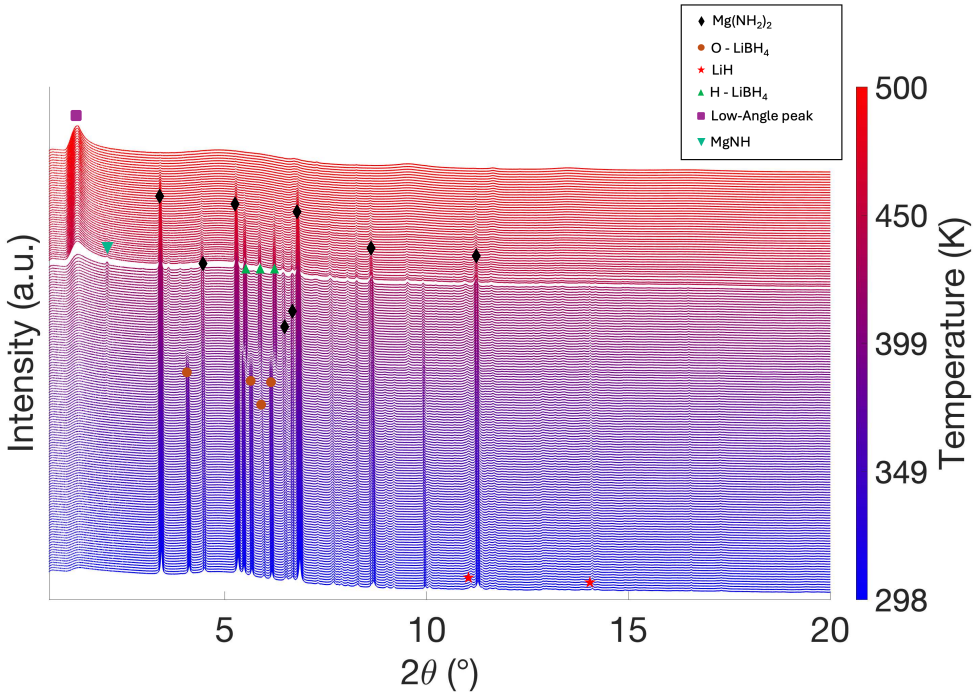


*Figure 4: T-ramp SR-PXRD from 298 K to 500 K of 6-9-18, with the major peaks indexed including a low angle peak at 1.3° 2θ*

Phase composition analysis (Figure 5) showed that in the 6-9-12 system, $Mg(NH_2)_2$ and LiH reacted between 340–430 K with minimal hydrogen evolution. Above 440 K, $Mg(NH_2)_2$ appears to react with $LiBH_4$, leading to significant hydrogen release. MgNH formation began at 440 K and persisted throughout the thermal ramp, alongside the continued growth of the 1.3° peak. Weak diffraction peaks consistent with a $LiNH_2$–$LiBH_4$ compound were observed [21] but no crystalline $Li_4(BH_4)(NH_2)_3$ was detected under the current experimental conditions, unlike the 6-9-1 and 6-9-6 systems.

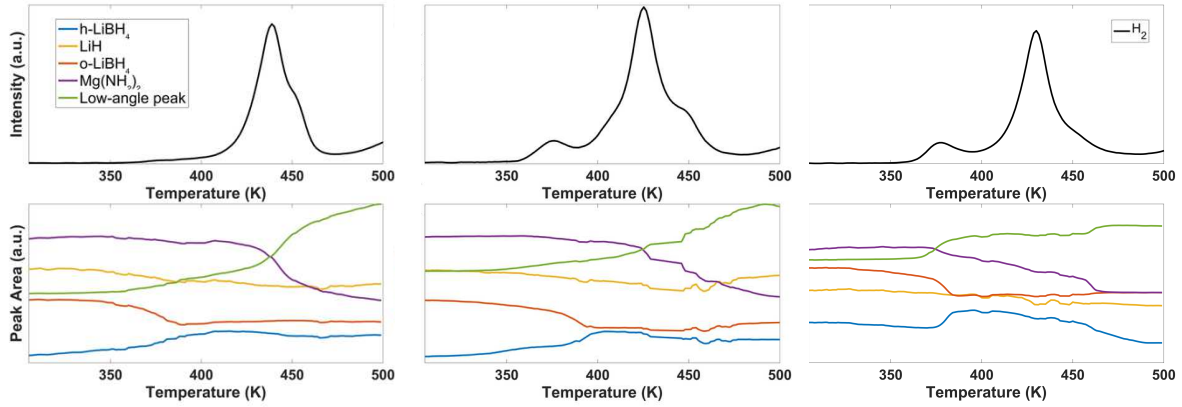


*Figure 5: Peak areas compared with $H_2$ MS data, utilised for understanding phase composition, in the 6-9-12 (left), 6-9-18 (middle) and 6-9-24 (right) systems. Low-angle peak refers to the unknown peak appearing at 1.3 °in the SR-PXRD measurements*

In the 6-9-18 system, LiH consumption began from ~330 K (Figure 5), with MgNH forming between 360–430 K but disappearing above 450 K. The transition from $Mg(NH_2)_2$–LiH to $Mg(NH_2)_2$- $LiBH_4$ reaction pathways occurred at ~430 K. In the 6-9-24 system, $Mg(NH_2)_2$ and

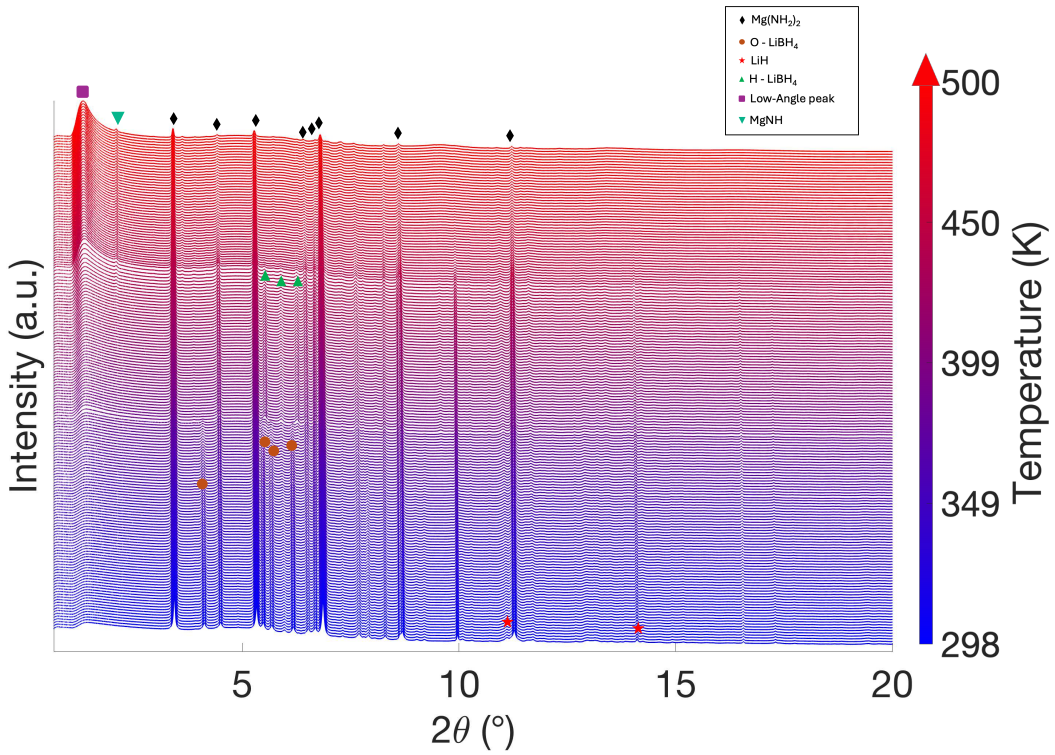


*Figure 6: T-ramped SR-PXRD from 298 K to 500 K of 6-9-12, with the major peaks indexed*

$LiBH_4$ reacted from 380 K, while LiH decreased more gradually. No MgNH formation was observed in the 6-9-24 system.

The low-angle peak at 1.3° (d-spacing = 15.63 Å) was consistently observed in the 6-9-6, 6-9-12, 6-9-18, and 6-9-24 compositions. There are no other reflections observed in the data for this phase, suggesting that this peak corresponds to a large superstructure with poor ordering. The growth of the low-angle peak in the SR-PXRD is correlated with hydrogen release and a decrease in $LiBH_4$ content (shown in Figure 5), indicating a partially decomposed Li–Mg–N–B–H intermediate which is either a layered or intercalated structure. Other possible explanations include nanoscale or amorphous phases, although the sharpness of the peak makes these less likely options, but they cannot be excluded totally. The low angle peak appears and then reduces as $Li_2Mg_2(NH)_3$ forms in the 6-9-6 composite and was also observed at the same d-spacing with other capillary materials during preliminary measurements at UCLouvain (Supporting Information, S2).

Alongside the low angle peak there are weak peaks relating to a primitive cubic cell ($Pm\bar{3}m$) with a lattice parameter of 3.02 Å (indexed in table 1 below) observed weakly from 450 K onwards in the 6-9-18 system. The peaks are seemingly separate to the low angle peak observed at 1.3°, and the peaks for this phase are very weak (SI S7) and are most prominent in the 6-9-18 system at 500 K, however these peaks can also be weakly observed in the 6-9-12 and 6-9-24 samples at 500 K.

*Table 1: Indexed PXRD pattern for the weakly observed primitive cell ($Pm\bar{3}m$) at 500 K, compared to a $Pm\bar{3}m$ cell with a lattice parameter of 3.02 Å*

| $2\theta_{obs}$ (°) | H K L | $2\theta_{calc}$ (°) | $2\theta_{obs}$ -$2\theta_{calc}$ (°) | $d_{obs}$ (Å) | $d_{calc}$ (Å) |
|---|---|---|---|---|---|
| 6.73 | 001 | 6.73 | –0.007 | 3.02 | 3.02 |
| 9.52 | 011 | 9.53 | –0.009 | 2.14 | 2.14 |
| 11.67 | 111 | 11.68 | –0.011 | 1.75 | 1.74 |
| 13.48 | 002 | 13.49 | –0.013 | 1.51 | 1.51 |
| 15.08 | 012 | 15.09 | –0.014 | 1.35 | 1.35 |
| 19.11 | 202 | 19.12 | -0.018 | 1.07 | 1.07 |
| 21.39 | 301 | 21.41 | –0.020 | 0.96 | 0.96 |
| 23.46 | 222 | 23.48 | –0.022 | 0.87 | 0.87 |

## 4. Discussion:

Here we report a step change in lowering the onset temperature of $H_2$ release by over 100 K compared to the original $6Mg(NH_2)_2 – 9$ LiH system without $LiBH_4$, accompanied by a corresponding new reaction pathway for the 6-9-18 and 6-9-24 systems, offering potential for improved cycling stability due to the lack of ammonia release. The thermal and structural analysis presented here reveals insights into the dehydrogenation of $Mg(NH_2)_2$–LiH–$LiBH_4$ RHCs and their further optimisation potential.

The 6-9-1 and 6-9-6 systems, despite their higher capacities, are not fully reversible. The 6-9-1, for example, has been shown to reduce to 96% capacity after 14 cycles, as well as showing a significant reduction in the kinetics by a factor of ca, 2.6 for the dehydrogenation reaction [41]. Gizer et al. demonstrated the cycling of 6-9-1 up to 20 times with a negligible drop in capacity, but they did note a similar reduction in the kinetics of the 6-9-1 system over the cycling [22]. The detection of $NH_3$ release above 473 K in the 6–9–1 composite, with a temperature 30 K above the cycling temperature used by Gizer et al. [22], points to ammonia evolution as a likely contributor to the capacity degradation observed during cycling.

For the 6-9-6 system, the first dehydrogenation cycle contains a loss of ca. 1 wt%, with no observable release of $NH_3$ or $H_2$. The cause for this weight loss is not clear. It cannot at present not be excluded that in this sub-stoichiometric RHC boron related species such as diborane ($B_2H_6$) or borane ($BH_3$) are released as potential decomposition products of $LiBH_4$. Prior studies have shown that during the dehydrogenation of less stable borohydrides, desorbing at lower temperatures (below 473 K) release diborane, whereas more stable borohydrides that release at over 523 K preferentially release hydrogen [54–56]. This is due to diborane decomposing at ca. 523 K [57]. Both theoretical [58] and experimental studies [59] have shown previously that species like diborane can be formed in the dehydrogenation reactions of $LiBH_4$, although diborane is difficult to observe experimentally with mass spectrometry, requiring Raman spectroscopy [59].

Further evidence of boron species impacting reaction pathways is clear in the 6-9-6 system, where the in-situ SR-PXRD highlights distinct difference to the 6-9-1 system. At high temperatures after dehydrogenation, the 6-9-1 has two strong crystalline phases present, $Li_2Mg_2(NH)_3$ and $Li_4(BH_4)(NH_2)_3$. In the 6-9-6, only the $Li_2Mg_2(NH)_3$ phase is observed to be crystalline, with no evidence of the $Li_4(BH_4)(NH_2)_3$ phase or any other crystalline B-containing phase forming. This could be explained by preferential partial diborane or borane release earlier in the reaction mechanism or the formation of amorphous boron rather than forming $Li_4(BH_4)(NH_2)_3$ [53].

The 6-9-12 has been shown to have improved reversibility against the 6-9-1 and 6-9-6 systems [21,46], with a measured capacity of 2.66 wt% (Figure 2), consistent with the literature [21,46]. In the TGA data for the 6-9-12, there is no significant mass loss below 400 K, much like the 6-9-1 (Figure 2), although it has an earlier onset of hydrogen release at 368 K compared to 391 K the 6-9-1. Studies on the 6-9-12 however have shown release at 371 K over more than 140 hours [21], implying that kinetic limitations at lower temperatures prevent this system from ambient operation.

Here we report two novel systems, the 6-9-18 and 6-9-24, which both display significantly lower hydrogen desorption onset temperatures compared to previous 6-9-*x* composites, releasing $H_2$ from 350 K and 358 K respectively: ca. 100 K lower than the reported values of 458 K for the $Mg(NH_2)_2$ – LiH system without $LiBH_4$ [60]. In these novel systems the early hydrogen release (below 400 K) leads to a fast hydrogen release of 1.2 wt% for the 6-9-18 and 1 wt% for the 6-9-

24, compared to 0.2 wt% for the 6-9-12, Figure 2. The hydrogen MS signal is also much stronger below 400 K, illustrating a difference in reaction pathway from the 6-9-12 to the 6-9-18 and 6-9-24 samples, and further evidencing the key role of $LiBH_4$ concentration in modulating the dehydrogenation onset. Table 2 summarise the key observations for each of the systems. Initial testing (SI, S6) shows the 6-9-18 continues to be a reversible system when tested under PCI conditions, but further work is required to investigate if there is any reduction in capacity over multiple cycles (> 50). Similarly, the plateau of the curves at 400 K is around 100 bar which was the maximum of the experimental setup, further testing on higher pressure sieverts apparatus is required.

The multiple hydrogen release steps observed by the DSC and MS data (Figures 2 & 3) along with products in table 2 provides further evidence of the presence of distinct reaction pathways that are composition dependent. The large enthalpies, such as 74.2 J $g^{-1}$ for the first endothermic event in the 6-9-18 system, exceeds the expected value for the $LiBH_4$ phase transition [53]. This is seen across all the 6-9-*x* samples implying that additional reactions are occurring in this temperature range. The in-situ PXRD data supports the idea of additional reactions, with the emergence of a low-angle diffraction peak unaccounted for by known phase transitions. This feature likely corresponds to an intermediate, facilitating the low-temperature hydrogen release and potentially suppressing $NH_3$ evolution, a persistent challenge in nitrogen-based hydrides.

*Table 2: Phases observed via in-situ SR-PXRD of the 6-9-x systems*

| | $Li_2Mg_2(NH)_3$ | $Li_4(BH_4)(NH_2)_3$ | $MgNH$ | 1.3° Peak | $Pm\bar{3}m$ |
|---|---|---|---|---|---|
| 6-9-1 | Yes ca. 445 K. | Yes ca. 445 K | No | No | No |
| 6-9-6 | Yes ca. 450 K | No | No | Yes ca. 350 K, disappears ca. 450 K | No |
| 6-9-12 | No | No | Yes ca. 400 K | Yes ca. 350 K | Yes, ca. 420 K |
| 6-9-18 | No | No | Yes ca. 350 K, disappears ca. 420 K | Yes ca. 350 K | Yes, ca. 420 K |
| 6-9-24 | No | No | No | Yes ca. 350 K | Yes, ca. 420 K |

The 6-9-1 system, as mentioned above, follows a previously reported reaction pathway [22] forming $Li_2Mg_2(NH)_3$ and $Li_4(BH_4)(NH_2)_3$. In contrast, the 6-9-12 and 6-9-18 systems exhibit an apparent two-step mechanism: initial $Mg(NH_2)_2$–LiH reaction at lower temperatures, followed by $Mg(NH_2)_2$–$LiBH_4$ reactions at higher temperatures as evidenced by Figure 5. The persistence of MgNH in the 6-9-12 system and its disappearance in the 6-9-18 system suggests compositionally driven changes in reaction intermediates.

With the 6-9-24 system, the $LiBH_4$ content dominates the reaction pathway from the outset. The early interaction between $Mg(NH_2)_2$ and $LiBH_4$, coupled with minimal LiH involvement, suggests that once $LiBH_4$ exceeds a critical concentration, it controls the dehydrogenation mechanism. This may explain both the low-temperature release and the unique structural features observed.

The consistent observation of the 1.3° low-angle peak across $LiBH_4$ rich samples suggests the formation of a metastable superstructure like phase, previously unreported for such $Mg(NH_2)_2$–LiH–$LiBH_4$ systems. A previously reported low angle peak for an intermediate in the decomposition of $LiBH_4$ by Mosegaard et al. (called Phase I) showed a peak with a d-spacing of 13.50 Å (using λ = 0.92191 Å) which was unidentified [61]. This is different to the peak observed in the $LiBH_4$ rich samples here, where a low angle peak with a d-spacing of 15.63 Å (λ = 0.35472 Å) is observed. None of the other reflections associated with this peak in Phase I

were observed in the samples herein. In addition, the low angle peak observed by Mosegaard et al. [61] was reported to appear between 473 K and 573 K, whereas in the 6-9-18 system presented here, it is observed to begin from 388 K.

At 500 K in the *x*=18 and 24 composites, there are broad peaks over the region from ca. 4° – 7° 2$\theta$ indicating either a molten or amorphous phase. For the *x*=18 composite visual observations from heating in a round-bottom flask up to 480 K indicates that this is likely related to a molten phase. The onset temperature of these either amorphous or molten phases, alongside the metastable phases such as 1.3° low-angle peak may play a central role in promoting faster hydrogen release while preventing ammonia generation. Vajo et al [62,63] have shown that the presence of multiple solid phases in a material hinders the kinetics of the solid phase transformations that are key to hydrogen release. These solid-solid reactions can only occur when particles are in physical contact at the atomic scale, limiting the kinetics of the material as transport rates are often slow in solids. When a eutectic electrolyte, such as $0.725LiBH_4/0.275KBH_4$, is added the transport rates of the various species in the reaction improve as the ions can diffuse through the electrolyte, leading to an increase in the (de)hydrogenation reactions [63]. A potential explanation behind the reduction in the onset temperature for the *x*=18, 24 systems is that the molten or amorphous character and the 1.3° low-angle peak here are related to an unreported eutectic electrolyte that is being formed in-situ, increasing transport rates and lowering the kinetic barrier of the reaction, with the 6-9-18 system having the most optimal ratio of $LiBH_4$ for this electrolyte.

The observed primitive cubic cell with a lattice parameter of 3.02 Å, is unreported in previous experiments involving $6Mg(NH_2)_2$–9LiH–*x*$LiBH_4$ systems. Calcium-nitrogen systems have been investigated for research into ammonia synthesis, and a cubic structure for $Ca_2NH$ have been experimentally verified [64], however, there has never been a reported experimental observation of a similar $Mg_2NH$ phase, with a report from 2009 proposing it as a potential compound in complex hydride systems[29]. Initial observations from this data indicate a cubic structure observed in the 6-9-12, 6-9-18 and 6-9-24 samples after 420 K, we propose the cubic cell observed is $Mg_2NH$.

This primitive cubic cell, combined with the molten or amorphous character over the borohydride peaks between 4-7° 2$\theta$ and the superstructure like low angle peak at 1.3° offers interesting insights suggesting a different pathway from the 6-9-1 and 6-9-6 systems. From the data presented in this paper the most likely pathway is evidenced by the changing of Mg phases in the 6-9-18 sample compared to the 6-9-1, assuming the primitive cell is $Mg_2NH$:

Step 1: $6Mg(NH_2)_2 + 9\,LiH + 18LiBH_4 -> 6MgNH + A + yLiBH_4 + 9H_2$

Step 2: $6MgNH + yLiBH_4 + A -> 3Mg_2NH + A + B + 3.5H_2$

Where A is likely a superstructure containing Li-B-N-H. Above 420 K the SR-PXRD highlights the MgNH reaction with *y*LiBH4 to release hydrogen, forming structure B. B has broad peaks across the region where borohydride peaks lie, indicative of a molten borohydride phase. This is likely to be an ammoniated borohydride $Li(NH_3)_x(BH_4)$. This is plausible as we know from the literature that ammoniated $LiBH_4$ can be molten when x = 2 at room temperature, and when x = 1 it is molten at 331 K [65]. In the 6-9-18 and 6-9-24 systems molten phases are observed from 340 K, indicating that any $Li(NH_3)_x(BH_4)$ phase will have an x < 1. Preliminary experiments have indicated that the 6-9-18 sample has a conductance of 4 x$10^{-7}$ S $cm^{-1}$ at 303 K, assuming the conductivity is dominated by the ammoniated phase, this would mean x < 0.5, possibly as low as 0.2 compared to the literature[65]. If we assume x = 0.2 for an $Li(NH_3)_x(BH_4)$ phase as B then

working backwards through the mechanism, allows us to postulate an empirical formula for the large superstructure, A, based on a new two step pathway for the 6-9-18 system:

Step 1: $6Mg(NH_2)_2 + 9\,LiH + 18LiBH_4 -> 6MgNH + 3\,Li_4BN_2H_7 + 15LiBH_4 + 9H_2$

Step 2: $6MgNH + 15LiBH_4 + 3\,Li_4BN_2H_7 \longrightarrow 3Mg_2NH + 3\,Li_4BN_2H_7 + 15Li(NH_3)_{0.2}(BH_4) + 3.5H_2$

## 5. Conclusion:

In this work we report the so far lowest gas-phase reversible hydrogen release temperatures in Reactive Hydride Composites, showing the potential of further optimisation of such storage materials for hydrogen storage applications even at ambient working temperatures. We demonstrate that increasing the $LiBH_4$ content well beyond the traditionally explored regime leads to qualitatively new behaviour in $Mg(NH_2)_2$- LiH - $LiBH_4$ Reactive Hydride Composites. The 6-9-18 and 6-9-24 compositions exhibit fundamentally different reaction pathways, distinct from all previously reported lower-ratio systems, and these new pathways enable the lowest gas-phase reversible hydrogen-release temperatures achieved to date in RHCs. This highlights the potential for off-board and on-board hydrogen storage applications for these materials.

Most notably, synchrotron PXRD reveals two entirely new intermediate phases, neither of which has been previously identified in RHC chemistry despite two decades of investigation. The evidence of two prior unreported phases, a large superstructure, and a primitive cubic cell represents a step-change in our understanding of how high $LiBH_4$ environments restructure the amide-hydride reaction landscape. These phases do not appear, and were not predicted, in any lower $LiBH_4$ systems, underscoring that high borohydride loading drives new chemistry rather than perturbing existing pathways. We propose that this novel primitive cell is an unreported $Mg_2NH$ phase, analogous to the $Ca_2NH$ phase observed [64].

Crucially, these newly accessed phases provide previously unseen dehydrogenation routes that (i) dramatically suppress onset temperatures to as low as ~350 K, and (ii) avoid $NH_3$ release; a dual advance not achieved simultaneously in earlier RHC formulations. The ~100 K downward shift in onset temperature for 6–9–18 compared to the borohydride-free 6–9 composition demonstrates that $LiBH_4$ does not merely modify kinetics: at these higher concentrations, it functions as a structurally active reagent that defines the entire reaction sequence.

These findings highlight a powerful design principle: increasing $LiBH_4$ beyond conventional levels does not simply optimise known reactions but unlocks new phases, new mechanisms, and new performance regimes. Careful compositional tuning enables access to new reaction pathways and intermediate phases that promote low-temperature, high-capacity hydrogen storage. This establishes a clear rationale for pursuing high-borohydride RHCs as a distinct subclass of hydrogen-storage materials with properties inaccessible to 6-9–1 or 6-9-6 compositions. Importantly, initial cycling tests performed using a manual Sieverts apparatus confirm that the 6-9-18 composition is reversible, as shown in Supplementary Section S6, providing early experimental validation that these new pathways can support practical hydrogen uptake and release.

To fully exploit these discoveries, future work must examine long-term cycling stability (> 50 cycles) and resolve the structures of the newly observed phases using neutron diffraction, Pair Distribution Function analysis to unravel the amorphous phases, and complementary spectroscopy. Nevertheless, the present results demonstrate that rational compositional tuning

can yield reversible hydrogen release below 400 K, bringing RHC materials closer to meeting the >3 wt% target for practical, near-ambient hydrogen-storage applications.

**Acknowledgements:**
We would like to thank William Boardman and Timothy P Cooper for their support in the maintenance of the Nottingham laboratories. We would also like to thank Timothy Steenhaut and the team at ID22 for the ESRF beamtime provided under the proposal CH-7093. Funding and support were provided by the Leverhulme Trust under grant LIP-2021-018. This work was also supported by Engineering and Physical Sciences Research Council (EPSRC) [grant numbers EP/W005131/1, EP/W016656/1].

**Author contributions:**
*Nicholas Hall: Conceptualisation; Methodology; Investigation; Data Curation; Formal Analysis; Writing – Original Draft.*

*Jacob Prosser: Investigation; Data Curation; Writing – Review & Editing; Conceptualization.*

*Jamie Ramshaw: Investigation; Writing – Review & Editing.*

*Luke Woodliffe: Supervision; Investigation; Data Curation; Formal Analysis; Writing – Review & Editing.*

*Sweta Munshi: Formal Analysis; Writing – Review & Editing.*

*Muhammad Saad Salman: Supervision; Formal Analysis.*

*Guillaume Esser: Investigation (Synchrotron PXRD); Writing – Review & Editing.*

*Sanliang Ling: Supervision; Formal Analysis; Writing – Review & Editing.*

*Marek Polanski: Investigation (Reactive Milling); Writing – Review & Editing.*

*Yaroslav Filinchuk: Investigation (Synchrotron PXRD); Writing – Review & Editing.*

*Hujun Cao: Investigation (Magnesium Amide Synthesis); Writing – Review & Editing.*

*Ping Chen: Investigation (Magnesium Amide Synthesis); Writing – Review & Editing.*

*Martin Dornheim: Supervision; Conceptualisation; Methodology, Writing – Review & Editing.*

*David Grant: Supervision; Investigation; Data Curation; Formal Analysis; Conceptualization; Writing – Review & Editing.*

**Data Availability:**
All data is available on request. The raw unprocessed SR-PXRD data from ESRF can be found at the following DOIs:

*6-9-1 data can be found here*: https://doi.org/10.15151/ESRF-DC-2234133904
*6-9-6 data can be found here*: https://doi.org/10.15151/ESRF-DC-2234133069
*6-9-12 data can be found here*: https://doi.org/10.15151/ESRF-DC-2234115947
*6-9-18 data can be found here*: https://doi.org/10.15151/ESRF-DC-2234130698
*6-9-24 data can be found here*: https://doi.org/10.15151/ESRF-DC-2234134335

**References:**


[1] DOE U. Materials Based Hydrogen Storage. Https://WwwEnergyGov/Eere/Fuelcells/Materials-Based-Hydrogen-Storage n.d. /www.energy.gov/eere/fuelcells/materials-based-hydrogen-storage (accessed August 8, 2024).

[2] Hwang HT, Varma A. Hydrogen storage for fuel cell vehicles. Curr Opin Chem Eng 2014;5:42–8. https://doi.org/10.1016/J.COCHE.2014.04.004.

[3] Schlapbach L, Züttel A. Hydrogen-storage materials for mobile applications. 2001.

[4] Abdin Z, Tang C, Liu Y, Catchpole K. Current state and challenges for hydrogen storage technologies. Towards Hydrogen Infrastructure: Advances and Challenges in Preparing for the Hydrogen Economy 2024:101–32. https://doi.org/10.1016/B978-0-323-95553-9.00012-1.

[5] Züttel A. Hydrogen storage methods. Naturwissenschaften 2004;91:157–72. https://doi.org/10.1007/s00114-004-0516-x.

[6] Rusman NAA, Dahari M. A review on the current progress of metal hydrides material for solid-state hydrogen storage applications. Int J Hydrogen Energy 2016;41:12108–26. https://doi.org/10.1016/J.IJHYDENE.2016.05.244.

[7] Pierri E, Cirillo V, Vietor T, Sorrentino M. Adopting a Conversion Design Approach to Maximize the Energy Density of Battery Packs in Electric Vehicles 2021;14:1939. https://doi.org/10.3390/en14071939.

[8] Luo Y, Wu Y, Li B, Mo T, Li Y, Feng SP, et al. Development and application of fuel cells in the automobile industry. J Energy Storage 2021;42:103124. https://doi.org/10.1016/J.EST.2021.103124.

[9] Concept, Design and Manufacture of a Prototype Hydrogen Storage Tank Based on Sodium Alanate 2009. https://doi.org/10.1002/ceat.200900095.

[10] Züttel A, Wenger P, Rentsch S, Sudan P, Mauron P, Emmenegger C. LiBH4 a new hydrogen storage material. J Power Sources 2003;118:1–7. https://doi.org/10.1016/S0378-7753(03)00054-5.

[11] Ding Z, Li S, Zhou Y, Chen Z, Yang W, Ma W, et al. LiBH4 for hydrogen storage - New perspectives. Nano Materials Science 2020;2:109–19. https://doi.org/10.1016/J.NANOMS.2019.09.003.

[12] Li C, Peng P, Zhou DW, Wan L. Research progress in LiBH4 for hydrogen storage: A review. Int J Hydrogen Energy 2011;36:14512–26. https://doi.org/10.1016/J.IJHYDENE.2011.08.030.
[13] Orimo S, Nakamori Y, Kitahara G, Miwa K, Ohba N, Towata S, et al. Dehydriding and rehydriding reactions of LiBH4. J Alloys Compd 2005;404–406:427–30. https://doi.org/10.1016/J.JALLCOM.2004.10.091.
[14] Song Y, Yang R. Decomposition mechanism of magnesium amide Mg(NH2)2. Int J Hydrogen Energy 2009;34:3778–83. https://doi.org/10.1016/J.IJHYDENE.2009.03.016.
[15] Leng H, Pan Y, Li Q, Chou KC. Effect of LiH on hydrogen storage property of MgH2. Int J Hydrogen Energy 2014;39:13622–7. https://doi.org/10.1016/J.IJHYDENE.2014.02.131.
[16] Dematteis EM. Progress in Energy Hydrogen storage in complex hydrides: past activities and new trends 2022. https://doi.org/10.1088/2516-1083/ac7499.
[17] Xie L, Li Y, Yang R, Liu Y, Li X. Superior hydrogen desorption kinetics of Mg(NH2)2 hollow nanospheres mixed with MgH2 nanoparticles. Appl Phys Lett 2008;92:231910. https://doi.org/10.1063/1.2943284.
[18] Bösenberg U, Kim JW, Gosslar D, Eigen N, Jensen TR, von Colbe JMB, et al. Role of additives in LiBH4–MgH2 reactive hydride composites for sorption kinetics. Acta Mater 2010;58:3381–9. https://doi.org/10.1016/J.ACTAMAT.2010.02.012.
[19] Price TEC, Grant DM, Legrand V, Walker GS. Enhanced kinetics for the LiBH4:MgH2 multi-component hydrogen storage system – The effects of stoichiometry and decomposition environment on cycling behaviour. Int J Hydrogen Energy 2010;35:4154–61. https://doi.org/10.1016/J.IJHYDENE.2010.02.082.
[20] Wei J, Leng H, Li Q, Chou KC. Improved hydrogen storage properties of LiBH4 doped Li–N–H system. Int J Hydrogen Energy 2014;39:13609–15. https://doi.org/10.1016/J.IJHYDENE.2014.02.130.
[21] Wang H, Wu G, Cao H, Pistidda C, Chaudhary A-L, Garroni S, et al. Near Ambient Condition Hydrogen Storage in a Synergized Tricomponent Hydride System 2017. https://doi.org/10.1002/aenm.201602456.
[22] Gizer G, Puszkiel J, Cao H, Pistidda C, Le TT, Dornheim M, et al. Tuning the reaction mechanism and hydrogenation/dehydrogenation properties of 6Mg(NH2)2-9LiH system by adding LiBH4. Int J Hydrogen Energy 2019;44:11920–9. https://doi.org/10.1016/j.ijhydene.2019.03.133.
[23] Dornheim M, Doppiu S, Barkhordarian G, Boesenberg U, Klassen T, Gutfleisch O, et al. Hydrogen storage in magnesium-based hydrides and hydride composites. Scr Mater 2007;56:841–6. https://doi.org/10.1016/J.SCRIPTAMAT.2007.01.003.
[24] Chen P, Xiong Z, Luo J, Lin J, Tan KL. Interaction of hydrogen with metal nitrides and imides 2002. https://doi.org/10.1038/nature01210.
[25] Barkhordarian G, Klassen T, Dornheim M, Bormann R. Unexpected kinetic effect of MgB2 in reactive hydride composites containing complex borohydrides. J Alloys Compd 2007;440:L18–21. https://doi.org/10.1016/J.JALLCOM.2006.09.048.
[26] Ibikunle AA, Sabitu ST, Goudy AJ. Kinetics and modeling studies of the CaH2/LiBH4, MgH2/LiBH4, Ca(BH4)2 and Mg(BH4)2 systems. J Alloys Compd 2013;556:45–50. https://doi.org/10.1016/J.JALLCOM.2012.12.144.

[27] Zeng L, Miyaoka H, Ichikawa T, Kojima Y. Superior Hydrogen Exchange Effect in the MgH 2-LiBH 4 System n.d. https://doi.org/10.1021/jp1042443.
[28] Karimi F, Pranzas PK, An J, Puszkiel A, María M, Riglos VC, et al. A comprehensive study on lithium-based reactive hydride composite (Li-RHC) as a reversible solid-state hydrogen storage system toward potential mobile applications † 2021. https://doi.org/10.1039/d1ra03246a.
[29] Pinkerton FE, Meyer MS, Meisner GP, Balogh MP, Vajo JJ, Mg T. Phase Boundaries and Reversibility of LiBH 4 /MgH 2 Hydrogen Storage Material 2025. https://doi.org/10.1021/jp0742867.
[30] Bergemann N, Pistidda C, Uptmoor M, Milanese C, Santoru A, Emmler T, et al. A new mutually destabilized reactive hydride system: LiBH4–Mg2NiH4. Journal of Energy Chemistry 2019;34:240–54. https://doi.org/10.1016/J.JECHEM.2019.03.011.
[31] Luo W. (LiNH2–MgH2): a viable hydrogen storage system. J Alloys Compd 2004;381:284–7. https://doi.org/10.1016/J.JALLCOM.2004.03.119.
[32] Markmaitree T, Osborn W, Shaw LL. Comparisons between MgH2- and LiH-containing systems for hydrogen storage applications. Int J Hydrogen Energy 2008;33:3915–24. https://doi.org/10.1016/j.ijhydene.2007.10.052.
[33] Markmaitree T, Shaw LL. Synthesis and hydriding properties of Li2Mg(NH)2. J Power Sources 2010;195:1984–91. https://doi.org/10.1016/J.JPOWSOUR.2009.09.067.
[34] Rijssenbeek J, Gao Y, Hanson J, Huang Q, Jones C, Toby B. Crystal structure determination and reaction pathway of amide–hydride mixtures. J Alloys Compd 2008;454:233–44. https://doi.org/10.1016/J.JALLCOM.2006.12.008.
[35] Nakamori Y, Kitahara G, Miwa K, Ohba N, Noritake T, Towata S, et al. Hydrogen storage properties of Li–Mg–N–H systems. J Alloys Compd 2005;404–406:396–8. https://doi.org/10.1016/J.JALLCOM.2004.10.089.
[36] Chen Y, Wu CZ, Wang P, Cheng HM. Structure and hydrogen storage property of ball-milled LiNH2/MgH2 mixture. Int J Hydrogen Energy 2006;31:1236–40. https://doi.org/10.1016/J.IJHYDENE.2005.09.001.
[37] Leng HY, Ichikawa T, Hino S, Hanada N, Isobe S, Fujii H. New Metal-N-H System Composed of Mg(NH 2 ) 2 and LiH for Hydrogen Storage 2004. https://doi.org/10.1021/jp048002j.
[38] Chen XY, Guo YH, Yu XB. Enhanced Dehydrogenation Properties of Modified Mg(NH 2 ) 2-LiBH 4 Composites n.d. https://doi.org/10.1021/jp1075753.
[39] Cao H, Pistidda C, Victoria M, Riglos C, Chaudhary A-L, Capurso G, et al. Conversion of magnesium waste into a complex magnesium hydride system: Mg(NH2)2-LiH † 2020. https://doi.org/10.1039/c9se01284b.
[40] Xiong Z, Wu G, Hu J, Chen P. Ternary imides for hydrogen storage. Advanced Materials 2004;16:1522–5. https://doi.org/10.1002/adma.200400571.
[41] Cao H, Wu G, Zhang Y, Xiong Z, Qiu J, Chen P. Effective thermodynamic alteration to Mg(NH 2 ) 2-LiH system: achieving near ambient-temperature hydrogen storage † 2014. https://doi.org/10.1039/c4ta03505d.
[42] Nakamori Y, Kitahara G, Orimo S. Synthesis and dehydriding studies of Mg–N–H systems. J Power Sources 2004;138:309–12. https://doi.org/10.1016/J.JPOWSOUR.2004.06.026.

[43] Xiong Z, Hu J, Wu G, Chen P, Luo W, Gross K, et al. Thermodynamic and kinetic investigations of the hydrogen storage in the Li–Mg–N–H system. J Alloys Compd 2005;398:235–9. https://doi.org/10.1016/J.JALLCOM.2005.02.010.
[44] Hu J, Liu Y, Wu G, Xiong Z, Chua YS, Chen P. Improvement of hydrogen storage properties of the Li-Mg-N-H system by addition of LiBH4. Chemistry of Materials 2008;20:4398–402. https://doi.org/10.1021/cm800584x.
[45] Zhang Y, Xiong Z, Cao H, Wu G, Chen P. The enhanced hydrogen storage performance of (Mg–B–N–H)-doped Mg(NH2)–2LiH system. Int J Hydrogen Energy 2014;39:1710–8. https://doi.org/10.1016/J.IJHYDENE.2013.11.008.
[46] Wang H, Cao H, Claudiop ], Garroni S, Wu G, Klassen T, et al. Hydrogen Storage Effects of Stoichiometry on the H2-Storage Properties of Mg(NH2)2-LiH-LiBH4 Tri-Component Systems n.d. https://doi.org/10.1002/asia.201700287.
[47] DOE USA. US DOE Hydrogen Energy Targets 2020-2025 2017. https://www.energy.gov/eere/fuelcells/downloads/target-explanation-document-onboard-hydrogen-storage-light-duty-fuel-cell. (accessed February 5, 2024).
[48] Baran A, Knioła M, Rogala T, Polanski M. New horizon in mechanochemistry—high-temperature, high-pressure mechanical synthesis in a planetary ball mill—with magnesium hydride synthesis as an example. Int J Hydrogen Energy 2022;47:35003–16. https://doi.org/10.1016/J.IJHYDENE.2022.08.080.
[49] Wyrębska I, Tomczyk K, Siemiaszko D, Zasada D, Dworecka-Wójcik J, Pęska M, et al. Spontaneous room temperature reaction of titanium and its alloys with hydrogen during self-shearing reactive milling. Chemical Engineering Journal 2024;485:149673. https://doi.org/10.1016/J.CEJ.2024.149673.
[50] Andrew Fitch, Ezio Covacci, Catherine Dejoie, Giorgia Confalonieri, Ola Grendal, Laurent Claustre, et al. ID22 – the high-resolution powder-diffraction beamline at ESRF. J Synchrotron Radiat 2023;5.
[51] Hammersley AP. FIT2D: A multi-purpose data reduction, analysis and visualization program. J Appl Crystallogr 2016;49:646–52. https://doi.org/10.1107/S1600576716000455.
[52] Rodríguez-Carvajal J. Recent advances in magnetic structure determination by neutron powder diffraction. Physica B Condens Matter 1993;192:55–69. https://doi.org/10.1016/0921-4526(93)90108-I.
[53] Ley MB, Roedern E, Jensen TR. Eutectic melting of LiBH4–KBH4. Phys Chem Chem Phys 2419;16:24194. https://doi.org/10.1039/c4cp03207a.
[54] Friedrichs O, Remhof A, Hwang S. Role of Li 2 B 12 H 12 for the Formation and Decomposition of LiBH 4. Chem Mater 2010;22:3265. https://doi.org/10.1021/cm100536a.
[55] Grochala W, Edwards PP. Thermal Decomposition of the Non-Interstitial Hydrides for the Storage and Production of Hydrogen 2004. https://doi.org/10.1021/cr030691s.
[56] Nakamori Y, Li HW, Matsuo M, Miwa K, Towata S, Orimo S. Development of metal borohydrides for hydrogen storage. Journal of Physics and Chemistry of Solids 2008;69:2292–6. https://doi.org/10.1016/J.JPCS.2008.04.017.
[57] So¨derlund MS, Ma¨ki-Arvela M, Era¨nen KE, Salmi T, Rahkola R, Murzin DY. Catalyst deactivation in diborane decomposition n.d. https://doi.org/10.1007/s10562-005-8690-9.

[58] Hoang K, Van De Walle CG. Mechanism for the decomposition of lithium borohydride. Int J Hydrogen Energy 2012;37:5825–32. https://doi.org/10.1016/J.IJHYDENE.2012.01.002.
[59] Reed D, Book D. Recent applications of Raman spectroscopy to the study of complex hydrides for hydrogen storage. Curr Opin Solid State Mater Sci 2011;15:62–72. https://doi.org/10.1016/J.COSSMS.2010.12.001.
[60] Wang J, Li H, Wang S, Liu X, Li Y, Jiang L. The desorption kinetics of the Mg(NH2)2 + LiH mixture. Int J Hydrogen Energy 2009;34:1411–6. https://doi.org/10.1016/J.IJHYDENE.2008.11.038.
[61] Mosegaard L, Møller B, Jørgensen JE, Bösenberg U, Dornheim M, Hanson JC, et al. Intermediate phases observed during decomposition of LiBH4. J Alloys Compd 2007;446–447:301–5. https://doi.org/10.1016/J.JALLCOM.2007.03.057.
[62] Vajo JJ, Tan H, Ahn CC, Addison D, Hwang S-J, White JL, et al. Electrolyte-Assisted Hydrogen Storage Reactions. J Phys Chem C 2018;122:2025. https://doi.org/10.1021/acs.jpcc.8b08335.
[63] Vajo JJ, Uddin J, Hwang S-J, Graetz J. Electrolytes in Multiple-Phase Hydrogen Storage Reactions 2023;11:267. https://doi.org/10.3390/inorganics11070267.
[64] Irvine GJ, Smith RI, Jones MO, Irvine JTS. Order-disorder and ionic conductivity in calcium nitride-hydride n.d. https://doi.org/10.1038/s41467-023-40025-2.
[65] Zhang T, Wang Y, Song T, Miyaoka H, Shinzato K, Miyaoka H, et al. Ammonia, a Switch for Controlling High Ionic Conductivity in Lithium Borohydride Ammoniates. Joule 2018;2:1522–33. https://doi.org/10.1016/J.JOULE.2018.04.015.

## Supplementary Files

This is a list of supplementary files associated with this preprint. Click to download.

- SupportinginformationTowardsambienttemperaturereversiblehydrogenstorageincomplexhydrides.pdf